Experimental characterization of the TCV dual-frequency gyrotron and validation of numerical codes including the effect of After Cavity Interaction

Jérémy Genoud[1*], *Stefano* Alberti[1], *Jean-Philippe* Hogge[1], *Konstantinos* Avramidis[2], *Falk* Braunmüller[1], *Alessandro* Bruschi[3], *Wiliam* Bin[3], *Jérémie* Dubray[1], *Damien* Fasel[1], *Gerd* Gantenbein[4], *Saul* Garavaglia[3], *Timothy* Goodman[1], *Stefan* Illy[4], *Jianbo* Jin[4], *François* Legrand[5], *Rodolphe* Marchesin[5], *Ioannis* Pagonakis[6], *Ugo* Siravo[1], and *Matthieu* Toussaint[1]

[1]Ecole Polytechnique Fédérale de Lausanne (EPFL), Swiss Plasma Center (SPC), Lausanne, CH-1015 Switzerland.
[2]Department of Physics, NKUA, Athens, Greece
[3]Istituto per la Scienza e la Tecnologia dei Plasmi (ISTP), Consiglio nazionale delle Riccerche, Milan, Italy
[4]IHM, Karlsruhe Institute of Technology, 76131 Karlsruhe, Germany.
[5]Microwave Imaging Solution, THALES, Vélizy-Villacoublay, F-78141, France.
[6]Department of Chemistry and Applied Biosciences, Eidgenössisch Technische Hochschule Zürich, Switzerland

Abstract. A dual-frequency gyrotron has been developed within the context of the recent Tokamak à Configuration Variable (TCV) upgrade. The gyrotron is designed to generate a 1 MW, 2 seconds RF wave at 84 or 126 GHz. Before integrating the gyrotrons in the TCV tokamak ECRH system, an extensive characterization of their behaviour has been performed. This paper focuses on presenting the results of these experiments at the two operating frequencies. The power measurements are systematically compared with numerical simulations. This comparison highlights the validation of numerical codes and the effect of After Cavity Interaction (ACI), a crucial factor that must be considered for achieving a good agreement between theoretical predictions and experimental results.

1 Introduction

The Tokamak à Configuration Variable (TCV) at the Swiss Plasma Center (SPC) in Lausanne underwent a significant upgrade of its heating system [1], involving the installation of two 1 MW, 30 keV D-beam injectors, and two 1 MW dual frequency 84/126 GHz gyrotrons. This upgrade aims to enhance both electron cyclotron heating but also direct ion heating in plasma experiments.

Developped collaboratively by SPC, the Karlsruher Institut für Technologie (KIT) and Thales Electron Devices, the dual-frequency gyrotron represents a remarkable achievement [2]. SPC and KIT performed the gyrotron design, while Thales ensured its manufacturing. Two gyrotrons have already been successfully integrated into the TCV tokamak Electron Cyclotron Resonance Heating (ECRH) system, and are efficiently exploited in the physics program. Following the success of this project, a third gyrotron has been recently ordered and will be operational in the first quarter of 2025.

2 Gyrotron design

The gyrotron is designed to generate 1 MW, 2 seconds of RF waves at either 84 GHz or 126 GHz, corresponding to the second (X2) or third cyclotron harmonics (X3) in TCV. The pulse duration is limited by the TCV maximum plasma duration.

A picture of the gyrotron is shown in Figure 1. The three mirror Matching Optics Unit (MOU) is located in the foreground of the photo, while the gyrotron is standing in the background. The first MOU mirror after the gyrotron window can be rotated to redirect the RF-beam either to the south-side (bottom right of the photo), in case of operation at 84 GHz or to the north side (left of the photo) for operation at 126 GHz. Each frequency has its own pair of focussing mirrors that couple the beam to the 63.5mm diameter waveguide.

The gyrotron design is based on the first W7-X gyrotron design [3–5], with modifications mainly to accommodate the multi-frequency operation. The approach was to optimize the design for the higher frequency, while maximizing the performance at the lower frequency. The main difference is the choice of a triode gun design, providing the necessary flexibility in the range of electron beam parameters. The cavity constant radius is slightly longer in order to increase the quality factor and efficiency at lower frequencies. A hybrid-type launcher has been designed to reach the highest Gaussian beam content. Since the gyrotron pulse length is limited to 2 s, a non-depressed collector enveloped by a longitudinal sweeping coil is used for the beam recovery system [6].

3 Experimental measurements

Before integration into the TCV tokamak's ECRH system, a phase of commissioning and characterization of their be-

*e-mail: jeremy.genoud@epfl.ch

Figure 1. Photo of the two dual-frequency gyrotrons installed in the TCV building. One of the Matching Optics Units is shown in the first plane of the picture.

haviour was performed. For this purpose, a load from the National Research Council (CNR)[7] is connected to the MOU output, through a set of transmission line (4 meters) and two miter bends. Each sub-component of the gyrotron has an independent cooling circuit equipped with input and output temperature sensors and flow-meters, allowing precise calorimetry. These tests demonstrated nearly identical performance of both gyrotrons. For the following discussions, only the results from the first gyrotron (on the left of the Figure 1) are presented.

For a typical operation at high-power, table 1 lists the gyrotron parameters for the two frequencies. For a good precision in the calorimetric measurement, a 500 ms pulse-length was considered. The corresponding calorimetric measurements are reported in table 2. The total losses in the MOU, in the two miter bends and in the transmission line has been considered to be 6%. With this value, the estimated power at the gyrotron window is 0.98 MW at 84 GHz and 1 MW at 126 GHz. The two operating points presented in this paper have been selected from a scan study in the frame of the comparison between experiments and simulations presented in the next section. They do not represent the tube's best performance. The gyrotron has demonstrated power in excess of 1 MW at both frequencies [2, 8]. The larger losses in the mirror box at 84 GHz are due to the larger diffraction losses on the internal mirrors at the lowest frequency. It is worth to note that no parasitic frequencies have been observed.

The power balance is achieved by comparing the power injected into the beam ($V_k \cdot I_k$) with the total power, which is the sum of the calorimetry measurement from each cooling circuit. Throughout the experimental campaign, the maximum error did not exceed 3%, underlining the reliability and precision of the test stand diagnostics.

Following the characterization of the gyrotrons' behaviour, the operating points for their operation on TCV have been selected. Additionally, since both gyrotrons are connected to the same Regulated High Voltage Power Supply (RHVPS), achieving similar performance at the same applied cathode voltage is convenient from the perspective of the ECH operator [9]. This was achieved by slightly tuning the magnetic field of both gyrotrons. In this way, operating points with power ranging from 400 kW to 950 kW were selected by varying, at each frequency, the cathode voltage only. The anode voltage power supply being very slow (20 ms rise-time), for fast modulation of the rf power (1 kHz), the cathode voltage is modulated.

Table 1. Experimental measurements.

Parameters	X2	X3
Mode	$TE_{17,5}$	$TE_{26,7}$
Magnetic field	3.28 T	4.94 T
Cathode voltage V_k	−79 kV	−77 kV
Anode voltage V_a	−44 kV	−56 kV
Beam current I_k	43.7 A	45 A
Frequency	83.8 GHz	125.9 GHz
Pulse length	500 ms	500 ms
P_{RF} at window	1MW	0.98 MW
Electronic efficiency	32%	30%

Table 2. Calorimetric measurements.

Parameters	Power [kW]	
	X2	X3
P_{cavity}	20	29
$P_{launcher}$	8	10
$P_{mirrorbox}$	87	57
$P_{collector}$	2366	2462
P_{load}	945	920
$P_{injected}$	3452	3430
P_{total}	3483	3533
Power balance error	0.9%	3%

4 Numerical calculations with TWANG

The gyrotron cavity interaction codes TWANG [10] or EURIDICE [11] have been used for the cavity design. Recently, it has been decided to compare TWANG simulations with the experimental measurements presented above. The numerical code TWANG [10], developed at SPC, is a non-linear code describing the wave-particle interaction for a single transverse TE mode. It has been used in combination with the code ARIADNE [12], a 3D self-consistent trajectory code utilized to calculate the beam parameters.

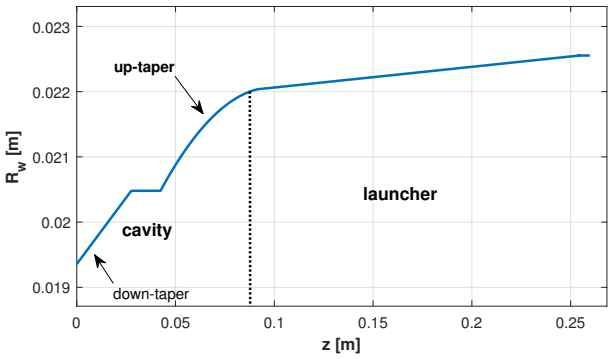

Figure 2. Cavity and launcher wall radius along the longitudinal direction z. The black dotted line indicates the separation between the "cavity only" interaction region and the launcher region. The "extended region" includes both the cavity and the launcher region (see text).

TWANG simulations were performed with the experimental parameters of eigh 500 ms pulses between V_k = 70 kV and V_k = 77 kV for the X3 operating point. The beam parameters at the entry of the cavity have been calculated accounting for a 50% beam space-charge neutralisation factor. The simulated RF powers generated in the cavity are shown with dashed lines in Figure 3.

This study considered three different interaction regions. Firstly the "cavity" interaction region, including the constant radius section, where the main interaction takes place, and the up-taper and down-taper as indicated in Figure 2. The numerical results with this interaction region are shown with the green dashed lines in Figures 3 and 4. They are to be compared with experimental powers shown as blue circles. Notably, the code underestimates the RF power for low cathode voltages and overestimates it at high values.

Subsequently, an "extended region" was considered, including both the cavity and the launcher in the simulation, as illustrated by the entire blue line in Figure 2. Simulated RF powers from this configuration, represented by the yellow dashed line in Figure 3, are in better agreement with the experimental measurements, particularly at low voltages. The overall shape of the curve is also in better agreement. The After Cavity Interaction (ACI)[13] is the physical mechanism leading to such an effect on the generated RF power. It is remarkable to note that this effect can have a positive or negative impact on the total RF power generation, as will be discussed in the following section.

Eventually, in order to include a more realistic geometry, the effect of thermal expansion of the cavity due to the wall loading was integrated in the geometry. The profile deformation is the result of a multi-physics simulation study involving gyrotron-interaction codes, but also thermal-hydraulic and thermo-mecanic models. Details of such studies have been reported in a recent publication [14]. In the following simulations, the deformation resulting from a high-power operating point at 1 MW was used. TWANG simulation results using the deformed cavity, along with the extended interaction region, are represented by the purple dashed line in Figure 3. The best agreement with experimental measurements is achieved with the deformed cavity configuration.

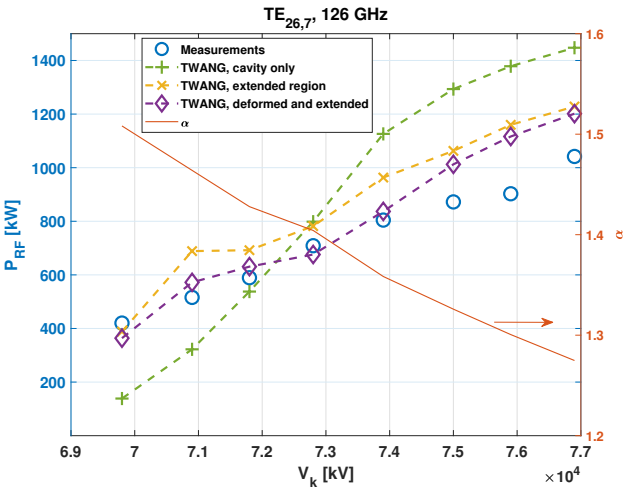

Figure 3. RF power at the output of the interaction region (or launcher) for the $TE_{26,7}$ mode at 126 GHz, measured by calorimetry (blue circles) or simulated with TWANG (dashed lines). Three different interaction regions are considered and described in the text. The pitch factor α value is indicated with the orange line.

A similar comparison has also been performed for the operating points at 84 GHz and the results are shown in Figure 4. For the deformed and extended interaction region, the result of a multi-physics simulations with the mode at 84 GHz has been used. The best agreement between experiments and simulations is found for an intermediate case in between the extended simulation region and the deformed and extended cavity simulation. However, it is noteworthy that below 75 kV, the TWANG code predicts a non-stationary operation, contrary to experimental observations. At these low voltages, the calculated pitch factor α(illustrated by the continuous orange line in Figures 3 and 4) exceeds 1.9, a significantly high-value where non-stationary oscillations could be anticipated. The discrepancy between experimental measurements and simulations for the low voltage operation at 84 GHz is currently being investigated.

5 After Cavity Interaction

As previously mentioned, the physical mechanism having an effect on the generated power in the launcher is the After Cavity Interaction. This effect is well known in the gyrotron community [13] and has already been the subject of numerical and experimental studies [15, 16]. This effect can either enhance or diminish the RF power generation. To illustrate this, it is worth focusing on the power balance between electron beam energy and EM wave energy, simulated along the extended interaction region.

Firstly, in Figure 5 c) the power balance is depicted for a simulation considering only the cavity region. It shows

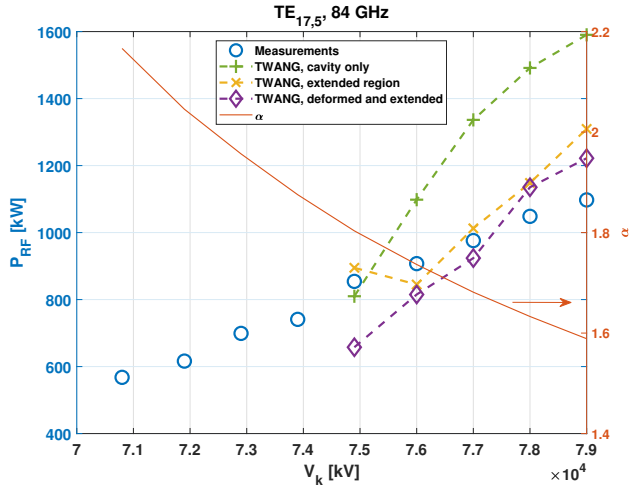

Figure 4. RF power at the output of the interaction region (or launcher) for the $TE_{17,5}$ mode at 84 GHz, measured by calorimetry (blue circles) or simulated with TWANG (dashed lines). Three different interaction regions are considered and described in the text. The pitch factor α value is indicated with the orange line.

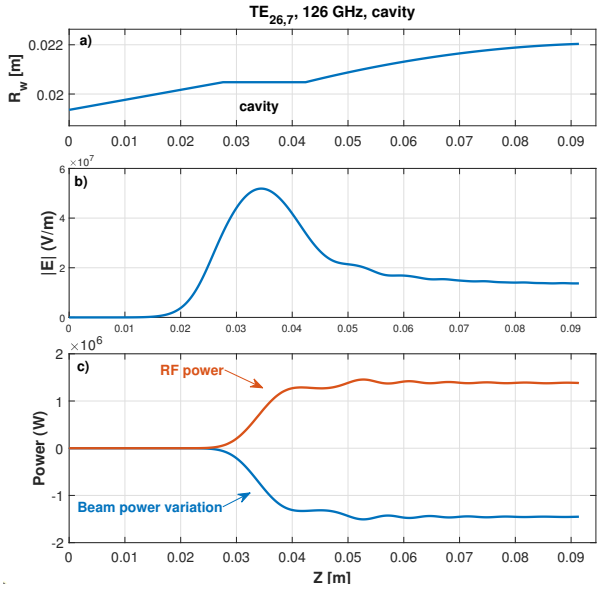

Figure 5. a) Schematic of the cavity radius along z. b) and c) Results from TWANG for the case $V_k = 75.9\,\mathrm{kV}$. b) Amplitude of the electric field profile along z. c) RF power (orange) and beam power (blue) along z.

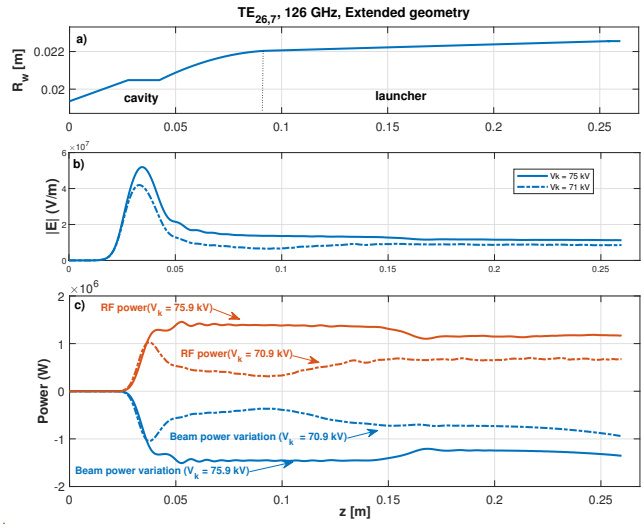

Figure 6. a) Schematic of the cavity radius along z. b) and c) Results from TWANG for the case $V_k = 75.9\,\mathrm{kV}$ (continuous line) and $V_k = 70.9\,\mathrm{kV}$ (dashed-dotted line). b) Amplitude of the electric field profile along z. c) RF power (orange) and beam power (blue) along z.

the electric field profile of mode $TE_{26,7}$, the RF power (P_{RF}) and the variation in the electron beam power (P_{beam}). The interaction occurs mainly in the constant radius section, where the resonant interaction leads to a net transfer of energy from the electron beam to the RF beam.

Next, Figure 6 portrays two simulations involving the extended region (cavity and launcher). The solid lines represent the simulation results from Figure 3 for for $V_k = 75.9\,\mathrm{kV}$ while the dashed lines correspond to the simulation results for $V_k = 70.9\,\mathrm{kV}$. The two contrasting effects of ACI are evident. For the higher voltage case, a second interaction occurs at $z = 0.16\,\mathrm{m}$, inside the launcher. This ACI is detrimental for the RF power generation, as it converts some of the electromagnetic wave power back into the electron beam power. Conversely, in the lower voltage scenario, the ACI is beneficial for the electromagnetic wave, by converting more of the electron beam power to the RF beam power. The interaction occurs over a more extended region in the launcher, from $z = 0.1\,\mathrm{m}$ to $z = 0.15\,\mathrm{m}$.

The ACI arises from a cyclotron resonance mechanism similar to that occuring in the main interaction region of the gyrotron. This resonance takes place when the relativistic cyclotron frequency of electrons is close to the frequency of the electromagnetic wave. Unlike the cavity region, the launcher area exhibits a lower magnetic amplitude but also a lower electron beam energy, resulting in potential resonant interactions. Figure 7 b) illustrates this phenomenon for the $V_k = 75.9\,\mathrm{kV}$ case of Figure 3. Both the cutoff frequency ω_{co} for the mode $TE_{26,7}$ (in blue) and the relativistic cyclotron frequency Ω_c (in orange) are shown with solid lines. The local average value of the electrons' energy has been used to calculate the relativistic cyclotron frequency. The crossing points of these curves indicate potential resonance locations. Two possible z position for the resonance are found. The first one at $z = 0.04\,\mathrm{mm}$, where the main interaction takes place and the second at $z = 0.145\,\mathrm{mm}$, close to the ACI region. It is noteworthy that this discussion relies on a first-order approximation, as the cutoff frequency represents the wave frequency only when $k_z = 0$, while ACI could involve waves with $k_z \neq 0$.

As a thought experiment, an additional simulation has been performed assuming a constant magnetic field after

the constant radius section of the cavity. The results of this simulation are depicted by dashed lines in Figure 7. For this special case, there is no resonance condition for ACI to develop according to Figure 7 b). Consequently, the power balance shown in Figure 7 c) demonstrates that RF power generated in the cavity remains unaffected in the launcher region. The RF power difference between these two cases is approximatively 200 kW.

This study underscores the effect of ACI on the RF power generation. A comprehensive analysis addressing the problem of ACI requires a more intricate study, involving in particular the consideration of magnetic field profile constraints to ensure both the safety and effective beam recovery in the collector region.

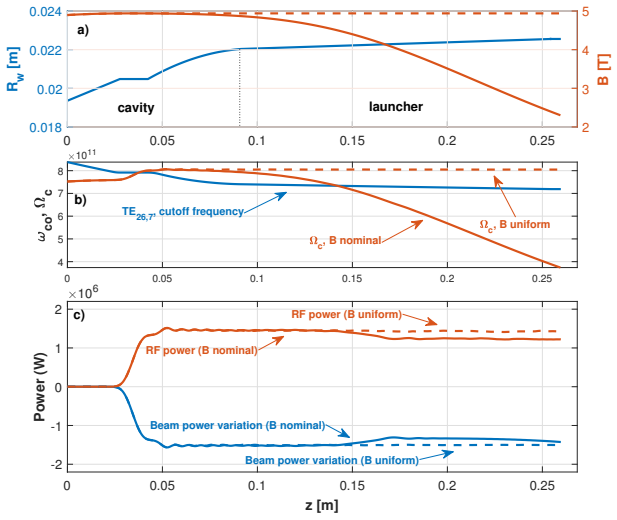

Figure 7. a) Schematic of the cavity radius along z. b) and c) Results from TWANG for the case $V_k = 75.9$ kV with nominal magnetic field profile (continuous line) and with an uniform profile after the cavity (dashed line). b) Amplitude of the electric field profile along z. c) RF power (orange) and beam power (blue) along z.

6 Conclusion

The development of two state-of-the-art dual frequency gyrotrons, each capable of delivering 1 MW of RF power, represents a successful collaboration between SPC, KIT and THALES Electron Devices. The two gyrotrons have been conditioned and extensively tested and their operation is a success for the electron cyclotron heating at TCV. This paper presents some of the experimental measurements, revealing calorimetric results with a power balance error lower than 3%. Moreover, simulations using the code TWANG have been compared with these measurements, showing a good qualitative agreement, allowing not only to validate the numerical tools employed at SPC but also to offer insights into the impact of after cavity interactions; in particular, it has been shown that ACI can either enhance or impede RF power generation.

ACKNOWLEDGMENTS

Work supported by the Ecole Polytechnique Fédérale de Lausanne (EPFL).

References

[1] A. Fasoli, for the TCV Team, Nuclear Fusion **55**, 043006 (2015)

[2] J.P. Hogge, S. Alberti, K.A. Avramidis, A. Bruschi, W. Bin, F. Cau, F. Cismondi, J. Dubray, D. Fasel, G. Gantenbein et al., AIP Conference Proceedings **2254**, 090006 (2020)

[3] S. Alberti, A. Arnold, E. Borie, G. Dammertz, V. Erckmann, P. Garin, E. Giguet, S. Illy, G. Le Cloarec, Y. Le Goff et al., Fusion Engineering and Design **53**, 387 (2001)

[4] M. Thumm, S. Alberti, A. Arnold, P. Brand, H. Braune, G. Dammertz, V. Erckmann, G. Gantenbein, E. Giguet, R. Heidinger et al., IEEE Transactions on Plasma Science **35**, 143 (2007), conference Name: IEEE Transactions on Plasma Science

[5] J. Jelonnek, F. Albajar, S. Alberti, K. Avramidis, P. Benin, T. Bonicelli, F. Cismondi, V. Erckmann, G. Gantenbein, K. Hesch et al., IEEE Transactions on Plasma Science **42**, 1135 (2014), conference Name: IEEE Transactions on Plasma Science

[6] J. Dubray, S. Alberti, D. Fasel, J.P. Hogge, P.F. Isoz, F. Legrand, M. Silva, U. Siravo, Fusion Engineering and Design **188**, 113410 (2023)

[7] W. Bin, A. Bruschi, F. Fanale, M. Francesca, F. Lucca, F. Albajar, S. Alberti, G. Carannante, M. Cavinato, I. Chelis et al., Fusion Engineering and Design **146**, 36 (2019)

[8] S. Alberti, K.A. Avramidis, W. Bin, A. Bertinetti, J. Dubray, D. Fasel, S. Garavaglia, J. Genoud, T. Goodman, J.P. Hogge et al., *High-efficiency, long-pulse operation of MW-level dual-frequency gyrotron, 84/126GHz, for the TCV Tokamak*, in *2019 44th International Conference on Infrared, Millimeter, and Terahertz Waves (IRMMW-THz)* (2019), pp. 1–2, iSSN: 2162-2035

[9] U. Siravo, S. Alberti, J. Dubray, D. Fasel, A. Perez, Fusion Engineering and Design **146**, 1510 (2019)

[10] S. Alberti, T.M. Tran, K.A. Avramides, F. Li, J.P. Hogge, 2011 36th International Conference on Infrared, Millimeter, and Terahertz Waves (irmmw-Thz) (2011)

[11] K.A. Avramides, I.G. Pagonakis, C.T. Iatrou, J.L. Vomvoridis, EPJ Web of Conferences **32**, 04016 (2012)

[12] J. Pagonakis, J. Vomvoridis, *The self-consistent 3D trajectory electrostatic code ARIADNE for gyrotron beam tunnel simulation*, in *Infrared and Millimeter Waves, Conference Digest of the 2004 Joint 29th International Conference on 2004 and 12th International Conference on Terahertz Electronics, 2004.* (2004), pp. 657–658

[13] V.E. Zapevalov, M.A. Moiseev, Radiophysics and Quantum Electronics **47**, 520 (2004)

[14] L. Savoldi, K.A. Avramidis, F. Albajar, S. Alberti, A. Leggieri, F. Sanchez, Energies **14**, 8027 (2021), number: 23 Publisher: Multidisciplinary Digital Publishing Institute

[15] E.M. Choi, M.A. Shapiro, J.R. Sirigiri, R.J. Temkin, Physics of Plasmas **14**, 093302 (2007)

[16] K.A. Avramidis, Z.C. Ioannidis, S. Illy, J. Jin, T. Ruess, G. Aiello, M. Thumm, J. Jelonnek, IEEE Transactions on Electron Devices **68**, 3063 (2021), conference Name: IEEE Transactions on Electron Devices